Cancer Letters 457 (2019) 1–9

Contents lists available at ScienceDirect

Cancer Letters

journal homepage: www.elsevier.com/locate/canlet

Original Articles

Tumor vasculature remodeling by radiation therapy increases doxorubicin distribution and efficacy

Vincent Potiron[a,b,1], Karen Clément-Colmou[a,b,1], Emmanuel Jouglar[a,b], Manon Pietri[a,b], Sophie Chiavassa[a,b], Grégory Delpon[a,b], François Paris[a,b], Stéphane Supiot[a,b,*]

[a] CRCINA, INSERM, Université de Nantes, Université D'Angers, Nantes, France
[b] Institut de Cancérologie de L'Ouest René Gauducheau, Saint-Herblain, France

Keywords:
Radiotherapy
Vascular normalization
Drug distribution
Chemotherapy
Pericyte

A B S T R A C T

The tumor microenvironment regulates cancer initiation, progression and response to treatment. In particular, the immature tumor vasculature may impede drugs from reaching tumor cells at a lethal concentration. We and others have shown that radiation therapy (RT) induces pericyte recruitment, resembling vascular normalization. Here, we asked whether radiation-induced vascular remodeling translates into improved tissue distribution and efficacy of chemotherapy.

First, RT induced vascular remodeling, accompanied by decreased hypoxia and/or increased Hoechst perfusion in prostate PC3 and LNCaP and Lewis lung carcinoma. These results were independent of the RT regimen, respectively 10×2 Gy and 2×12 Gy, suggesting a common effect. Next, using doxorubicin as a fluorescent reporter, we observed that RT improves intra-tumoral chemotherapy distribution. These effects were not hindered by anti-angiogenic sunitinib. Moreover, sub-optimal doses of doxorubicin had almost no effect alone, but significantly delayed tumor growth after RT.

These data demonstrate that RT favors the efficacy of chemotherapy by improving tissue distribution, and could be an alternative chemosensitizing strategy.

1. Introduction

Even in the current era of targeted therapies, the limited distribution of drugs remains a challenge [1]. This is due in part to the abnormal tumor vasculature, which has developed as a function of anarchic tumor expansion. The resulting network is tortuous, overbranched, variable in diameter and abnormally permeable [2,3]. All these factors contribute to reducing blood flow and consequently, the transport of therapeutic compounds. Independently, tumor cell density creates a compressive environment that blunts the endothelial lumen and limits extravasation of molecules because of high interstitial pressure [4]. Beyond drug distribution, the abnormal vasculature generates hypoxia and acidosis, leading to metabolism switch and the emergence of therapeutic resistances [5].

Hence, there is considerable need for a strategy to improve vascular function. The current literature places emphasis on vascular normalization [6], rather than on anti-angiogenic agents that can have limited efficacy [7,8]. Moreover, destructing angiogenesis or altering vascular maturation could favor metastasis [9–12]. Consequently, many drugs have been explored for their vascular normalizing potency [2,13,14].

To be sound from a clinical standpoint, such strategies should be as close as possible to existing practice. External radiotherapy (RT) is a standard treatment for about half of cancer patients, either alone or in combination with surgery and/or chemotherapy [15]. In general, RT is given as a fractionated regimen of about 2 Gy/day over a course of several weeks, to achieve a total dose of 40–80 Gy depending on tumor type and conformation. Recent advances in beam ballistics have enabled hypofractionated protocols whose biological responses remain largely unexplored. In particular, endothelial death after irradiation might be triggered only above ≈ 5–10 Gy [16].

Ultimately, RT leads to the destruction of target tissues. However, this process is gradual and allows time for complex biological phenomena to occur. We have previously shown in a xenograft prostate model that radiotherapy induces perivascular coverage of tumor microvessels [17]. This prompted us to investigate if RT favors intra-tumoral drug distribution. Anthracyclines such as doxorubicin are good

Abbreviations: Doxo, doxorubicin; MVD, microvascular density; RIVR, radiation-induced vascular remodeling; RT, radiation therapy

* Corresponding author. Institut de Cancérologie de l'Ouest René Gauducheau, Bvd Jacques Monod, 44800, Saint-Herblain, France.
E-mail address: stephane.supiot@ico.unicancer.fr (S. Supiot).

[1] These authors contributed equally to the work.

https://doi.org/10.1016/j.canlet.2019.05.005
Received 20 September 2018; Received in revised form 30 April 2019; Accepted 6 May 2019

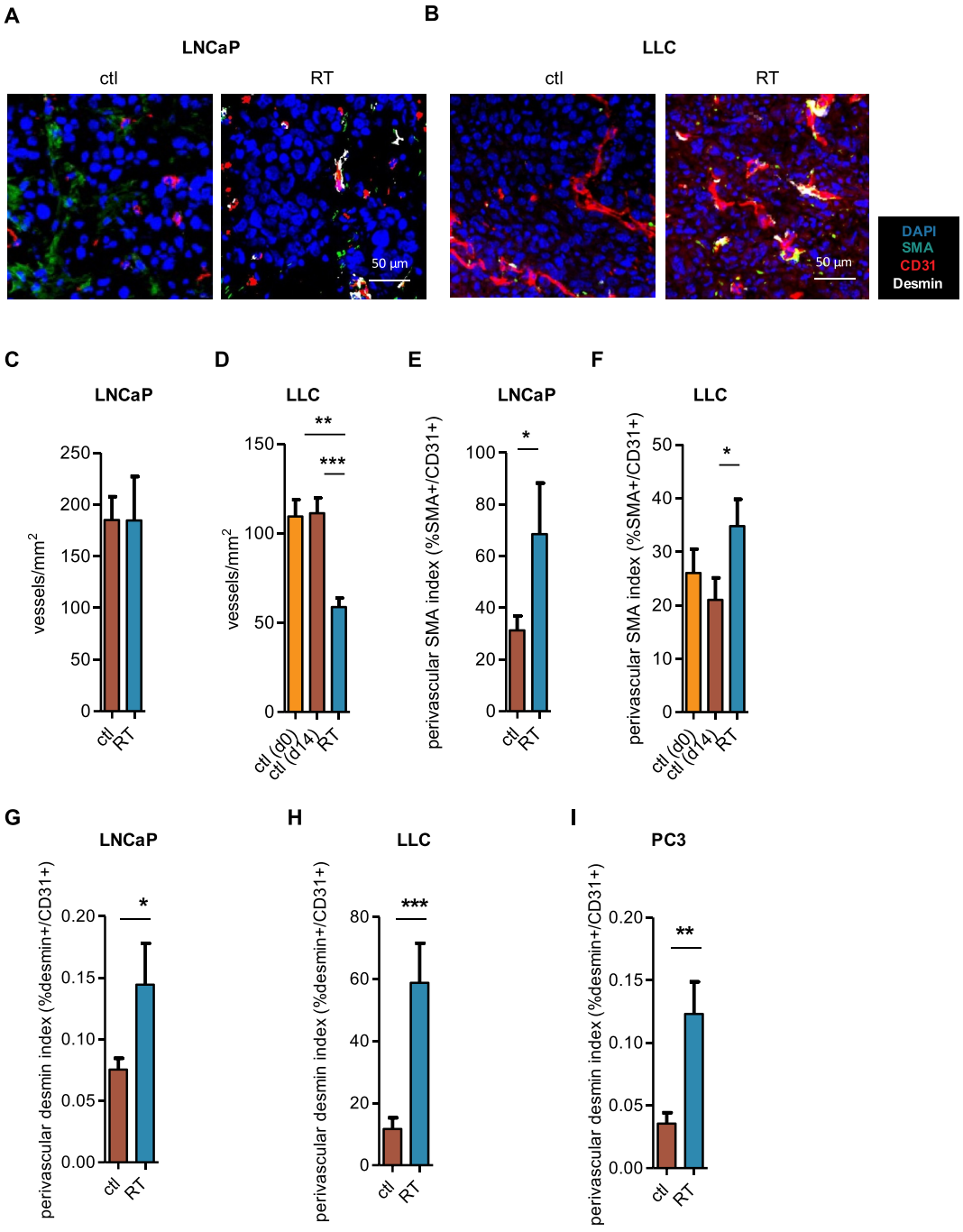

Fig. 1. RT induces vascular coverage. LNCaP tumors were engrafted orthotopically in NMRInu mice and irradiated at 10 × 2 Gy. LLC tumors were engrafted subcutaneously in C57B/L6 mice and irradiated at 2 × 12 Gy. After the two weeks of RT, animals were sacrificed and tumors were stained as indicated. A control group (ctl d0) was also collected before treatment for LLC. (A, B) representative scanner images of immunohistochemistry for endothelial cells (CD31) and pericytes (α-SMA/desmin) in LNCaP (A) and LLC (B) tumors. (C, D) CD31 $^{+}$ vessel density in LNCaP (C) and LLC (D) tumors. (E, F) quantification of α-SMA + area around CD31 $^{+}$ vessels in LNCaP (E) and LLC (F) tumors. (G–I) quantification of desmin + area around CD31 $^{+}$ vessels in LNCaP (G), LLC (H) and PC3 (I) tumors. (C–I) values represent the average of n ≥ 5 ± sem (LNCaP),n ≥ 7 (PC3) and ≥9 (LLC).

examples of chemotherapeutics for which tissue distribution greatly govern biological response *in vivo* [18]. Moreover, doxorubicin is naturally fluorescent in the range of 500–600 nm [19]. This made doxorubicin a stereotype candidate to study drug delivery. Indeed, vascular normalization has been shown to enhance doxorubicin accumulation [20,21].

In this study, we evaluated if 10 × 2 Gy and 2 × 12 Gy external X-ray irradiation induces a vascular normalization phenotype during which distribution and anti-tumor activity of the small molecule doxorubicin is more efficient, using prostate and lung xenograft models.

2. Materials and methods

2.1. Animal experiments

Prostate PC3 model: 6/8 week male NMRI-nude mice (Janvier, Saint Berthevin, France) were engrafted with subcutaneous injection of 2 × 10^6 PC3-luc cells (Caliper Life Sciences, Villepinte, France). Lewis lung carcinoma model: 6/8 week female C57BL/6 mice (Janvier, Saint Berthevin, France) were engrafted subcutaneously with 10^6 LLC cells (LL/2, LGC Standards, Molsheim, France). Tumor growth was measured

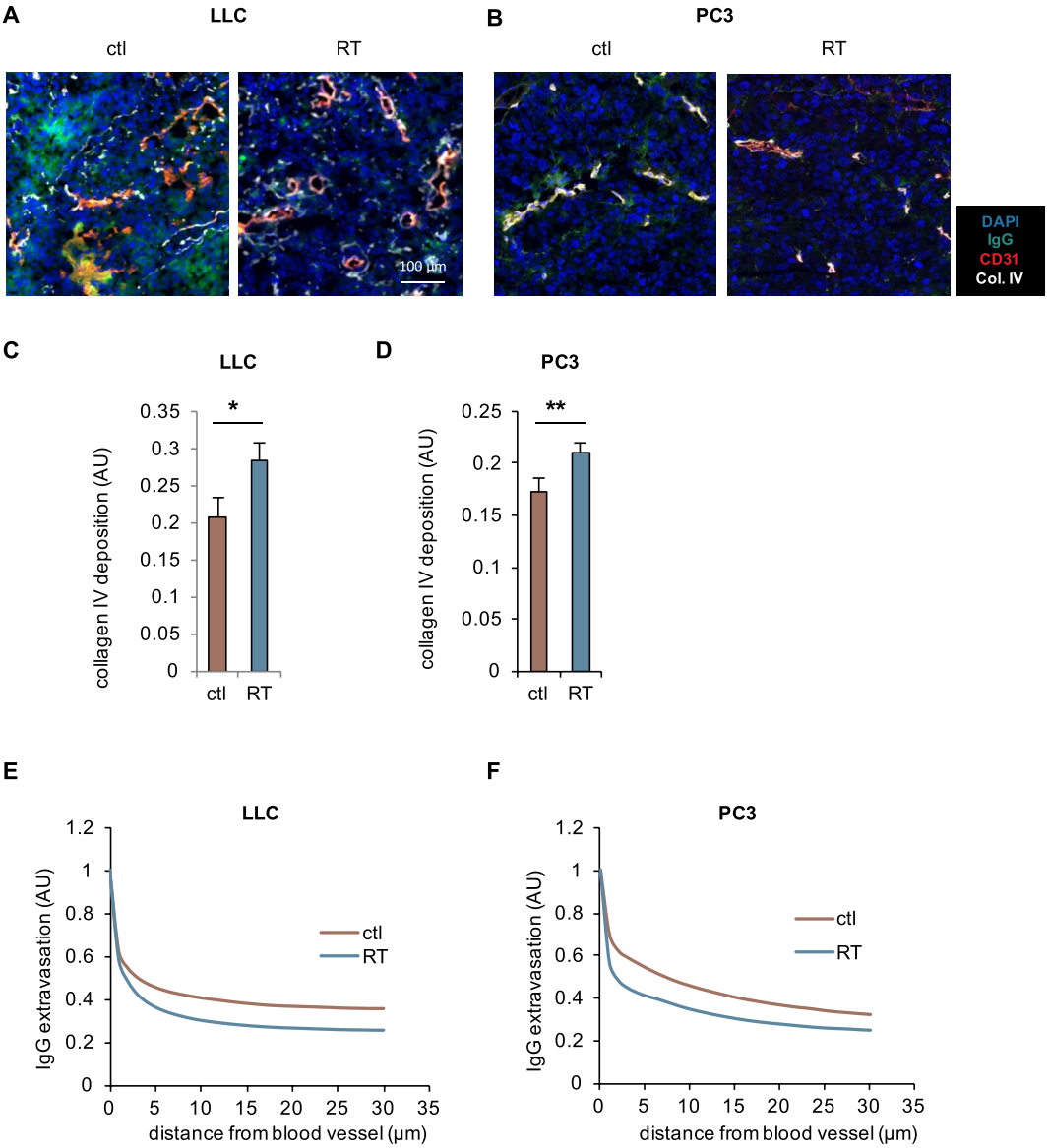

Fig. 2. RT increases basal membrane deposition and decreases IgG leakage. LLC tumors were engrafted subcutaneously in C57B/L6 mice and irradiated at 2 × 12 Gy. PC3 tumors were engrafted subcutaneously in NMRInu mice and irradiated at 10 × 2 Gy. After the two weeks of RT, animals were sacrificed and tumors were stained as indicated. (A, B) representative scanner images of LLC (A) and PC3 (B) tumors for basal membrane (collagen IV) and IgG leakage. (C, D) quantification of collagen IV deposition in the 5 µm around vessels in LLC (C) and PC3 (D) tumors. (E,F) quantification of IgG extravasation as a function of distance to the nearest blood vessel in LLC (E) and PC3 (F) tumors. (C–E) values represent the average of n ≥ 9 ± sem.

with a digital caliper ($v = 0.5*ab^2$ with a = largest diameter and b its perpendicular) and experiments begun when tumors reached ≈ 200 mm^3 (PC3: 3 weeks, LLC: 9 days). This size was chosen to reflect heterogeneous hypoxic tumors at the time of treatment. Prostate LNCaP model: 6/8 week male NMRI-nude mice were anesthetized with ketamine/xylazine (50/15 mg/kg) and 5 × 10^6 LNCaP-luc cells (Caliper Life Sciences) were injected in the left dorsolateral lobe of the prostate by laparotomy. Tumor uptake was followed weekly by luminescence using a PhotonImager (BiospaceLab, Paris, France) and groups with similar bioluminescence were formed (5 weeks). After sacrifice, tissues were frozen-embedded in OCT medium at −80 °C (Sakura Finetek, Villeneuve D'ascq, France). All experiments were done twice except for Fig. 7A and B n represents the number of animals and is indicated in the figure legends.

All animal experiments were carried out in accordance with the European Council Directive 2010/63/UE and approved by the local Animal Care and Use Committee (Comité d'Ethique en Expérimentation Animale des Pays-de-la Loire, C2EA-06) under protocols 01262.01, APAFIS 529, APAFIS 2336.

2.2. Radiation therapy

Irradiations were performed using a CP-160 X-ray irradiator (Faxitron, Lincolnshire, IL) with a 0.3 mm Cu filter, an accelerating voltage of 160 kV and a dose rate in the tumor of 1.3 Gy/min. Dose rate was determined according to the TG61 protocol [22] and from measurements in depth with a plane-parallel Roos ionization chamber (PTW GmbH, Freiburg, Germany) [23]. Animals received a dose of 2 Gy daily, 5 days per week (LNCaP, PC3) or 12 Gy weekly (LLC) for two weeks (= 10 × 2 Gy and 2 × 12 Gy), centered on the tumor-bearing region using lead shields.

2.3. Functional parameters and treatments

Hypoxia was evaluated by pimonidazole reactivity. Hundred µl of 70 µg/ml pimonidazole hydrochloride (Hypoxyprobe, Burlington, USA)

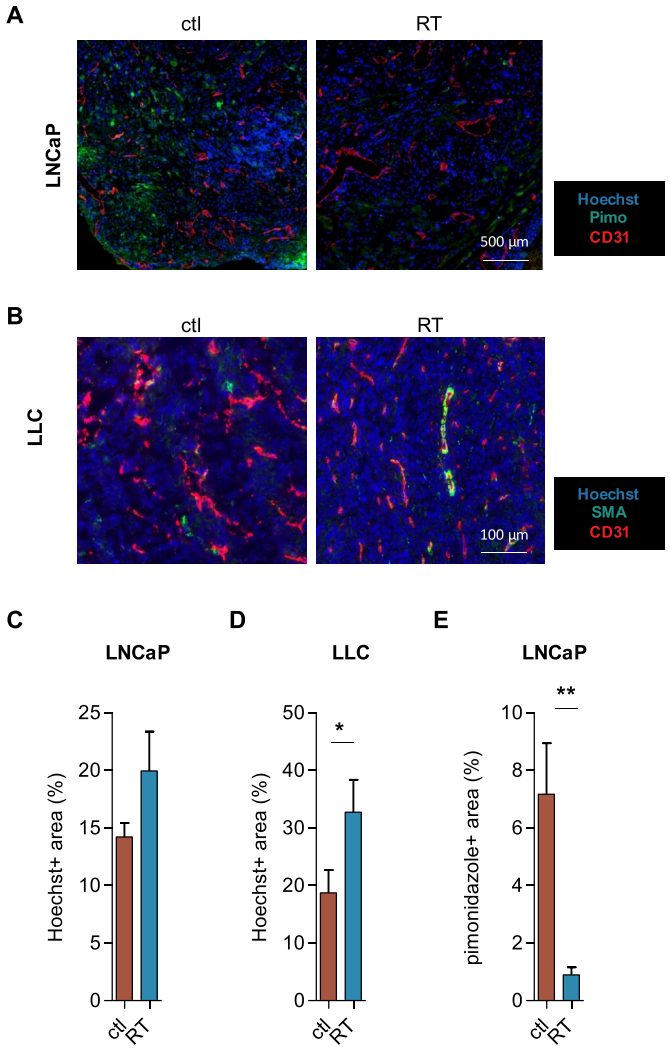

Fig. 3. RT induces increased perfusion and/or decreased hypoxia. LNCaP tumors were engrafted orthotopically in NMRInu mice and irradiated at 10 × 2 Gy. LLC tumors were engrafted subcutaneously in C57B/L6 mice and irradiated at 2 × 12 Gy. After the two weeks of RT, animals were injected with pimonidazole and Hoechst 33342, sacrificed and tumors were stained as indicated. (A, B) representative scanner images of LNCaP (A) and LLC (B) tumors injected with pimonidazole and/or Hoechst 33342. (C, D) quantification of Hoechst 33342 + area ratio to total tissue area in LNCaP (C) and LLC (D) tumors. (E) quantification of pimonidazole + area ratio to total tissue area in LNCaP tumors. (C–E) values represent the average of n ≥ 5 ± sem (LNCaP) and ≥9 (LLC).

was injected i.p. 2 h before sacrifice. Detection was performed by immunohistochemistry with FITC-conjugated antibody. Hoechst perfusion was evaluated by i.v. injection of 100 µl of 5 mg/ml Hoechst 33342 (Ozyme, Saint St-Quentin-en-Yvelines, France) 5 min before sacrifice. Doxorubicin distribution was assessed by i.v. injection of 100 µl of 18 mg/ml doxorubicin hydrochloride (Sigma, Saint-Quentin Fallavier, France) 5 min before sacrifice [19]. Detection was performed using a Nanozoomer HT fluorescence slide scanner (Hamamatsu Photonics, Massy, France) at 594 nm. Doxorubicin was given at 8 mg/kg i.p. for survival assays. Sunitinib was given per os at 40 mg/kg daily in pH 3.5 saline solution with 10% PEG300 [24].

2.4. Immunohistochemistry

Immunohistochemistry was performed using previously published staining procedures [17]. The following antibodies were used: rat anti-mouse CD31 (BD Biosciences, Le Pont-de-Claix, France), rabbit *anti*-desmin (Ozyme), rabbit anti-collagen IV(Life Technologies), Cy3-conjugated mouse anti-alpha smooth muscle actin (Sigma), Alexa^{647}-conjugated goat anti-rabbit, Alexa^{488}-conjugated goat anti-rat and Alexa^{488}-conjugated goat anti-mouse (Life Technologies). Slides were mounted in Prolong Gold with DAPI (Life Technologies) for nuclei counterstaining (except for the perfusion assays) and observed using a Nanozoomer slide scanner at 40x with fluorescence.

2.5. Image analysis

Analyses were performed on original 16-bit tiff images at 40x resolution using ImageJ 1.46r software (National Institutes of Health, USA) as previously described [17]. In brief, whole tumor images were segmented based on background/signal intensity and image features. Surfaces and count of positive objects were calculated in populated (DAPI+) tumor areas. Further details can be found in supplementary information.

2.6. Statistical analysis

Statistical analyses were performed using a two-tailed Mann-Whitney test with 95% confidence estimations, or a Kruskal-Wallis test with alpha risk = 0.05 followed by Dunn's post-test for multiple comparisons (GraphPad Prism5, La Jolla, California, USA). Pseudo-survival (morbidity) analyses were done by Kaplan-Meier curve and estimate. Data were considered significant at $p \leq 0.05$ (*), ≤ 0.01 (**) and ≤ 0.001(***).

3. Results

3.1. Radiotherapy improves vascular physiology in different tumor models

We have previously shown that standard fractionated irradiation (2 Gy/day) leads to coverage of the tumor endothelium by pericytes in a preclinical model of prostate cancer (PC3), characterized by α-SMA, NG2 and desmin expression and direct contact with endothelial cells [17]. We also observed that perfusion of dextrans was increased after two weeks of standard fractionated RT. To pursue these findings, we assessed two RT schemes using additional models: LNCaP (androgen-dependent prostate cancer, slow growing) and Lewis lung carcinoma (syngeneic C57BL/6 model, fast growing). Orthotopic luciferase-LNCaP derived tumors with a linear increase in bioluminescence (= 5 weeks post-graft) were irradiated daily using a standard 2 Gy dose Monday-Friday for two weeks (= 10 × 2 Gy). On the other hand, subcutaneous LLC tumors of ≈200 mm^3 were treated with a schedule of two 12 Gy fractions (each Monday for two weeks, = 2 × 12 Gy), since standard fractionation does not control tumor growth in this model (Clément-Colmou et al., submitted). Also, for LLC, two groups of controls were initially used to compare to tumors irradiated for two weeks (RT): “ctl d0" (first day of experiment) matched size and “ctl d14" (two weeks of experiment) matched age of the RT group. Because LNCaP (and PC3 later on) growth is slower, d14 controls were sufficient.

In the LNCaP model, 10 × 2 Gy RT did not reduce microvessel density (Fig. 1A,C). In the LLC model, 2 × 12 Gy RT limited microvessel density (−47%, $p < 0.001$, Fig. 1B,D). In both models, an increase in α-SMA positive mural cells was observed in the 2 µm region around endothelial cells (CD31$^+$) after two weeks of RT compared to non-irradiated tumors (LNCaP: +119%, $p = 0.05$, Fig. 1A,E; LLC, +65%, $p = 0.02$, Fig. 1B,F). Increased desmin staining, another marker for pericytes, was also evident in LNCaP, LLC and previously used PC3 cells after RT [17] (LNCaP: +92%, $p = 0.04$; LLC: +402%, $p = 0.0004$; PC3: +246%, $p = 0.005$) (Fig. 1A,B,G-I). There was no statistical difference between unirradiated LLC tumors harvested at d0 or d14 (Fig. 1D,F). Moreover, an increase in collagen IV in the basal membrane was noted (LLC: +37%, $p = 0.04$; PC3: +22%, $p = 0.007$) (Fig. 2A–D),

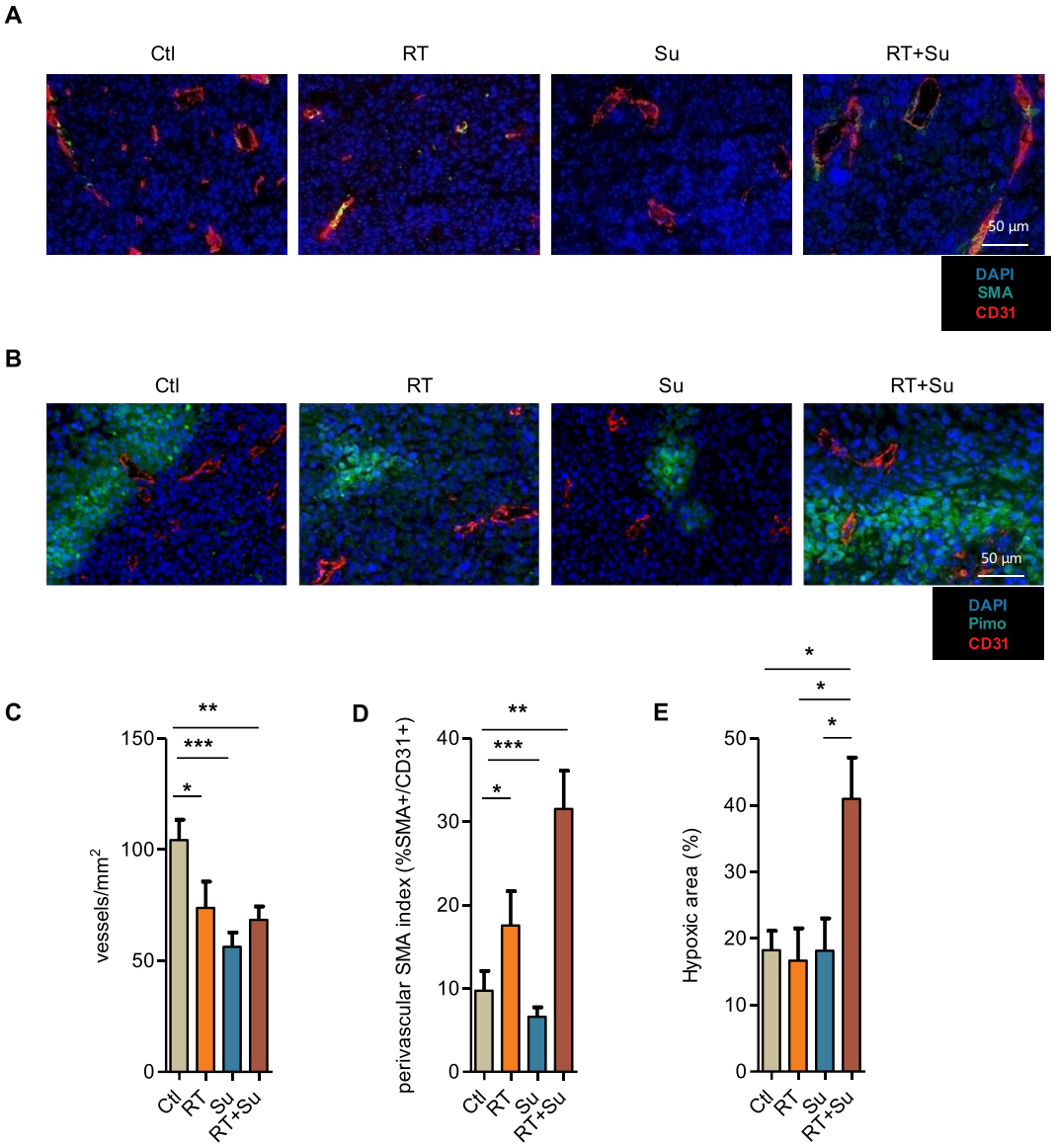

Fig. 4. RIVR is not affected by anti-angiogenic sunitinib in LLC tumors. LLC tumors were engrafted subcutaneously in C57B/L6 mice and irradiated at 2 × 12 Gy. During the two weeks of RT, animals were fed with sunitinib daily when indicated. Animals were injected with Hoechst 33342 before sacrifice and tumors were stained as indicated. (A) representative scanner images of immunohistochemistry for endothelial cells (CD31) and pericytes (α-SMA) in LLC tumors treated with RT, sunitinib or combination. (B) representative scanner images of LLC tumors injected with pimonidazole. (C) CD31 $^{+}$ vessel density in LLC tumors ± sunitinib. (D) quantification of α-SMA + area around CD31 $^{+}$ vessels in LLC tumors ± sunitinib. (E) quantification of pimonidazole area ratio to total tissue area in LLC tumors ± sunitinib. (C–E) values represent the average of n ≥ 13 ± sem.

suggesting vessel maturation. In parallel, extravasation of IgG, which are normally largely retained in the vessel lumen, was decreased after RT (LLC: 48%, p = 0.02; PC3: 33%, p = 0.04). This was evident starting from the first micrometers to the endothelial wall (Fig. 2E and F). At the functional level, RT slightly increased penetration of the Hoechst nuclear dye in LNCaP tumors (+40%, p = 0.08, Fig. 3A,C) and significantly favored its diffusion in LLC tumors (+75%, p = 0.04, Fig. 3B,D). Also, hypoxic area in pimonidazole-injected LNCaP tumors was greatly attenuated (−88%, p = 0.004, Fig. 3A,E). For all models (LLC, Figs. S1–2; PC3, Figs. S3–4; LNCaP, Fig. S5), changes were not correlated to either raw tumor size or size change. We have precedently used subcutaneous or orthotopic PC3 tumors with similar results ([17], Clément-Colmou et al., submitted). In addition, vascular remodeling was observed in both syngeneic (LLC) and immunocompromised (LNCaP, PC3) models. Collectively, these data indicate that RT generally improves vascular physiology in solid tumors after the first two weeks of treatment.

Radiotherapy is often combined with concomitant or neo-adjuvant chemotherapy. Anti-angiogenic compounds would be the most likely to affect radiotherapy-induced vascular remodeling (RIVR). We thus questioned if RIVR is robust and compatible with sunitinib, an EMA/FDA-approved inhibitor of the receptor tyrosine kinases VEGFR and PDGFR for which vascular normalization has been conflictually reported [25]. The LLC model was chosen because PC3 cells have been shown to respond to sunitinib, at least *in vitro* [26]. Mice bearing established LLC tumors were irradiated at 2 × 12 Gy and concomitantly fed daily with 40 mg/kg sunitinib or vehicle solution. After two weeks of treatment, vascular parameters were assessed as described above. Sunitinib reduced tumor microvessel density compared to control, in a similar manner to RT in that model (ctl: 104 vessels/mm^2, Su: 56, RT: 74, ctl vs RT p = 0.02; ctl vs Su p = 0.0001, Fig. 4A,C). The combination of RT + sunitinib did not further downregulate tumor microvessel density (RT + Su: 68, NS vs RT or Su). Moreover, sunitinib did not prevent perivascular coverage by α-SMA + cells (RT + Su: +224%

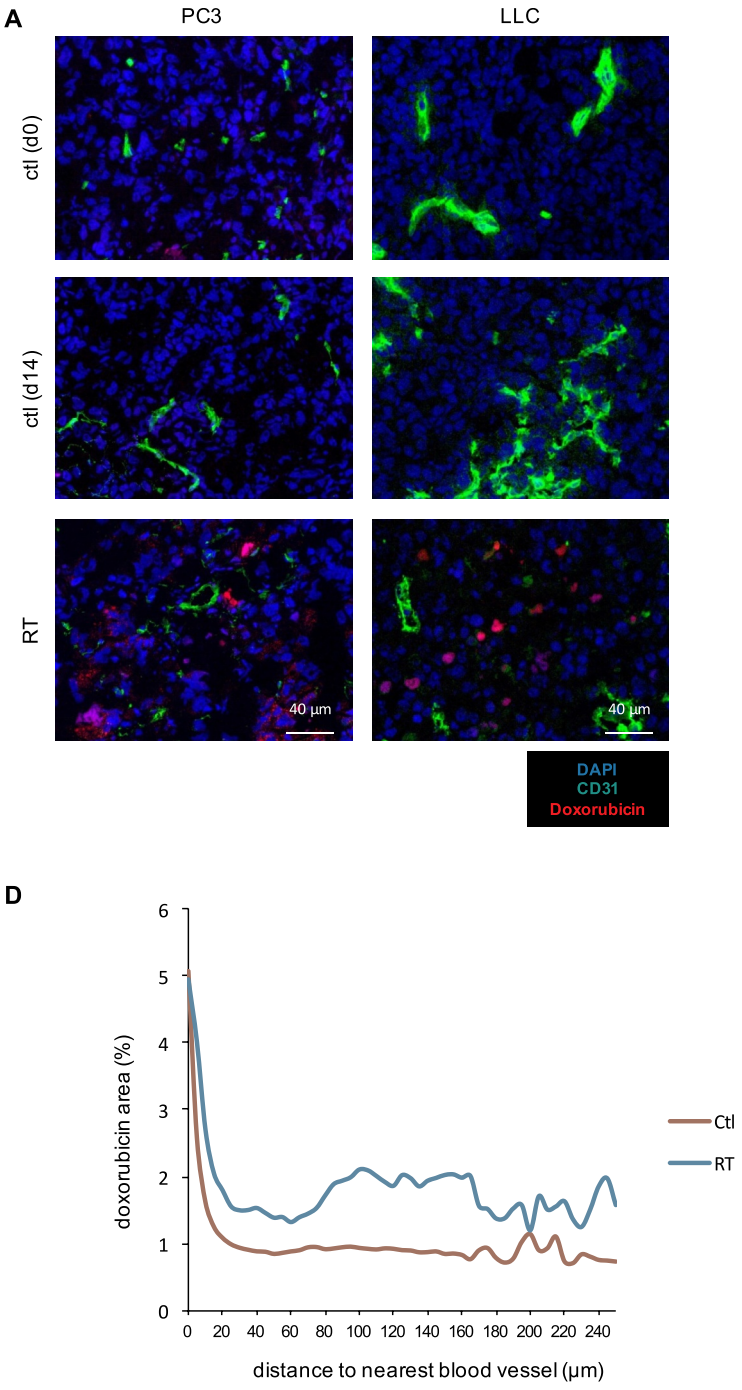

Fig. 5. RT improves intra-tumoral drug distribution. PC3 tumors were engrafted subcutaneously in NMRInu mice and irradiated at 10 × 2 Gy. LLC tumors were engrafted subcutaneously in C57B/L6 mice and irradiated at 2 × 12 Gy. After the two weeks of RT, animals were injected i.v. with doxorubicin, sacrificed and tumors were stained as indicated. A control group (ctl d0) was also collected before treatment. (A) representative scanner images of PC3 (left column) and LLC (right column) tumors injected with doxorubicin i.v. (B, C) quantification of doxorubicin area ratio to total tissue area in PC3 (B) and LLC (C) tumors. Values represent the average of n ≥ 9 ± sem. (D) plot profile of doxorubicin distribution as a function of distance to nearest vessel in PC3 tumors.

vs ctl, p < 0.0001, Fig. 4A,D). Nevertheless, we noted that combination of sunitinib + RT increased hypoxia (ctl: 18.2% area; RT + Su: 41%; +125%, p = 0.01; Fig. 4B,E).

3.2. Radiotherapy improves intra-tumoral diffusion of doxorubicin

To assess whether RIVR allows increased intra-tumoral accumulation of small molecule chemotherapy, we monitored distribution of doxorubicin (doxo). Established subcutaneous PC3 and LLC tumors were subjected to RT (respectively 10 × 2 Gy and 2 × 12 Gy) for two weeks, the period where remodeling of the vasculature is observed. Mice were then injected with 18 mg/kg doxorubicin i.v. and intra-tumoral distribution was assessed using fluorescence microscopy 5 min after injection [19]. Whereas doxorubicin was detected at low levels in control tumors, irradiated tumors displayed significantly higher drug accumulation (PC3: +331%, p = 0.006, Fig. 5A and B; LLC: +508%, p = 0.05 Fig. 5A,C). This was not due to tumor age or size since untreated LLC tumors collected at the beginning (ctl d0) or end (ctl d14) of RT planning had similarly low doxorubicin levels (Fig. 5A,C). Moreover, although RT slowed tumor growth (Fig. S6A), doxorubicin distribution was not correlated to tumor size (Fig. S6B).

The profile of doxorubicin distribution was consistent with that of a vascular-administrated drug, yielding high positivity close to blood vessels and diminishing with distance (Fig. 5D). Notably, RT increased doxorubicin content both close to and at distance from vessels, compared to control.

To extend the observation that sunitinib did not interfere with RIVR, doxorubicin area was assessed in the context of concomitant planning

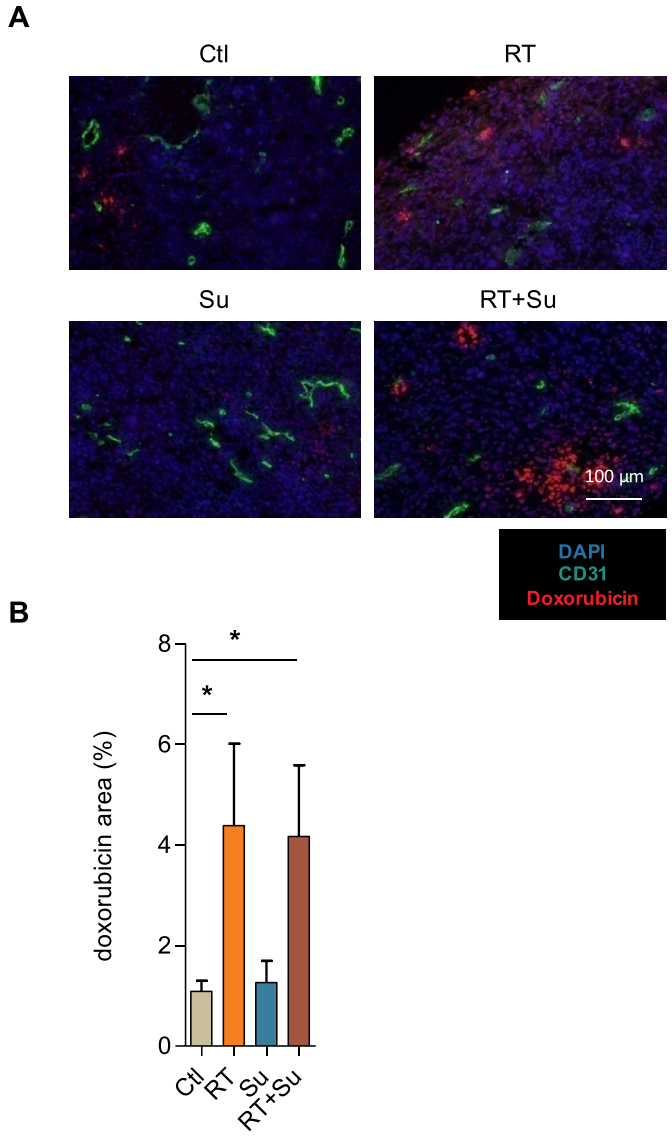

Fig. 6. Increased doxorubicin diffusion is not reversed by anti-angiogenic sunitinib. LLC tumors were engrafted subcutaneously in C57B/L6 mice and irradiated at 2 × 12 Gy. During the two weeks of RT, animals were fed with sunitinib daily when indicated. Animals were injected with doxorubicin i.v. before sacrifice and tumors were stained as indicated. (A) representative scanner images of LLC tumors injected with doxorubicin i.v. and treated with RT, sunitinib or combination. (B) quantification of doxorubicin area ratio to total tissue. Values represent the average of n ≥ 13 ± sem.

as precedently. As expected, RT increased drug distribution compared to control (ctl: 1.1% total area, RT: 4.4, p = 0.02; Fig. 6A and B). However, sunitinib had no effect alone (Su: 1.3%) and did not counteract RT-induced distribution (RT + Su: 4.4%, p = 0.02 vs ctl).

3.3. Radiotherapy improves doxorubicin efficacy

Chemotherapy effectiveness is strongly dependent on the dose that can be achieved in situ [27]. We thus questioned whether increased doxorubicin delivery is accompanied with higher drug efficacy. First, we performed a dose-response of doxorubicin on anti-tumor growth (Fig. 7A and B). Based on these results, 8 mg/kg i.p. was chosen as it is below the maximal dose of doxorubicin. Therefore, the expected increase in local drug concentration into the tumor after RT would be able to translate into higher efficacy. To investigate this, doxorubicin was administered on the beginning of week 3, thus at an interval (3d) after the last RT fraction to minimize biochemical radiosensitization. In the PC3 model, while doxorubicin barely affected tumor growth when delivered alone, treatment after RT induced a significant shift in morbidity compared to RT alone (median survival ctl: 43 days, doxo: 43 days, RT: 53.5 days, RT + doxo: 68 days, p < 0.0001, Fig. 7C). In the LLC model, doxorubicin administration after RT also delayed tumor growth better than when given alone (median survival ctl: 18 days, doxo: 23 days, RT: 24.5 days, RT + doxo: 33.5 days, p < 0.0001, Fig. 7D).

4. Discussion

Efficient diffusion of chemotherapeutics is a challenge that is currently under extensive exploration. For this purpose, the concept of vascular normalization has gained interest. In this study, we questioned if external radiotherapy, a standard anti-cancer treatment, could favor small molecule distribution and efficacy.

First, we show that external radiotherapy reproducibly improves vascular function in tumor models with different kinetics and different RT schedules, after two weeks of treatment. Secondly, we show that RT increases intra-tumoral doxorubicin diffusion. Thirdly, we show that doxorubicin delivered after radiotherapy has higher efficacy on tumor growth. Moreover, combination with anti-angiogenic sunitinib does not counteract RIVR nor drug delivery. Overall, these data establish a proof of concept that RIVR could be helpful for delivering cancer chemotherapeutics.

Radiotherapy has been shown to increase efficacy and distribution of liposomal doxorubicin in the context of concomitant treatment [28]. This is of interest, since chemotherapies are routinely used as radiosensitizing agents, but dosage is often limited due to toxicity of the combination. We show here that radiotherapy improves efficacy of chemotherapy later (3 days) after irradiation. Our results suggest that radiotherapy could be used to enhance local efficacy of chemotherapy in the target tumor without the need for concomitant planning and undesired toxicity. This would be expected to increase the benefit/risk ratio of chemotherapy/radiotherapy association. Such strategies could even be tested in radioresistant tumors for the sole purpose of increasing their sensitivity to chemotherapy. This might extend to larger molecules since enhancement of antibody uptake has been reported after RT [29]. Moreover, based on our data using sunitinib, anti-angiogenic drugs are compatible as well with the caveat of monitoring hypoxia. Interestingly, sunitinib itself has been shown to be more efficient after irradiation, although its distribution was not investigated [26]. Novel technologies now allow for non-invasive imaging of tumor oxygenation and vascular changes [30,31]. Thus, clinical trials testing the chemosensitizing properties of localized irradiation should monitor vascular parameters to identify the best timing for association with chemotherapy.

Penetration of molecules results from the combination of physical and biological factors relating to tumor cells, vessels and stroma [1]. Short-term (hours) after irradiation, vessels have been shown to react by increasing permeability [32,33]. Alternatively at later times, high-dose irradiation has been associated with vessel death [16,33] and decreased MVD [34,35]. However, decreased MVD is not systematic and there is also evidence for increased perfusion in long-term response to RT [17]. Based on the literature, it is likely that RT initially destabilizes vessel structure and selects established mature vessels (e.g. vascular pruning, hours), but induces vascular remodeling and pericyte recruitment in a second phase (days) during which vascular function is optimal. Additionally, parameters such as composition and stiffness of the extracellular matrix [36], pH, interstitial fluid pressure [37], density of tumor cells and repopulation time after RT [4] will also affect drug distribution. Thus, extensive research will be required to clarify which parameters are specifically affected by RT.

We have previously observed that fractionated daily 10 × 2 Gy RT leads to vascular coverage by α-SMA/desmin mural cells, decreased

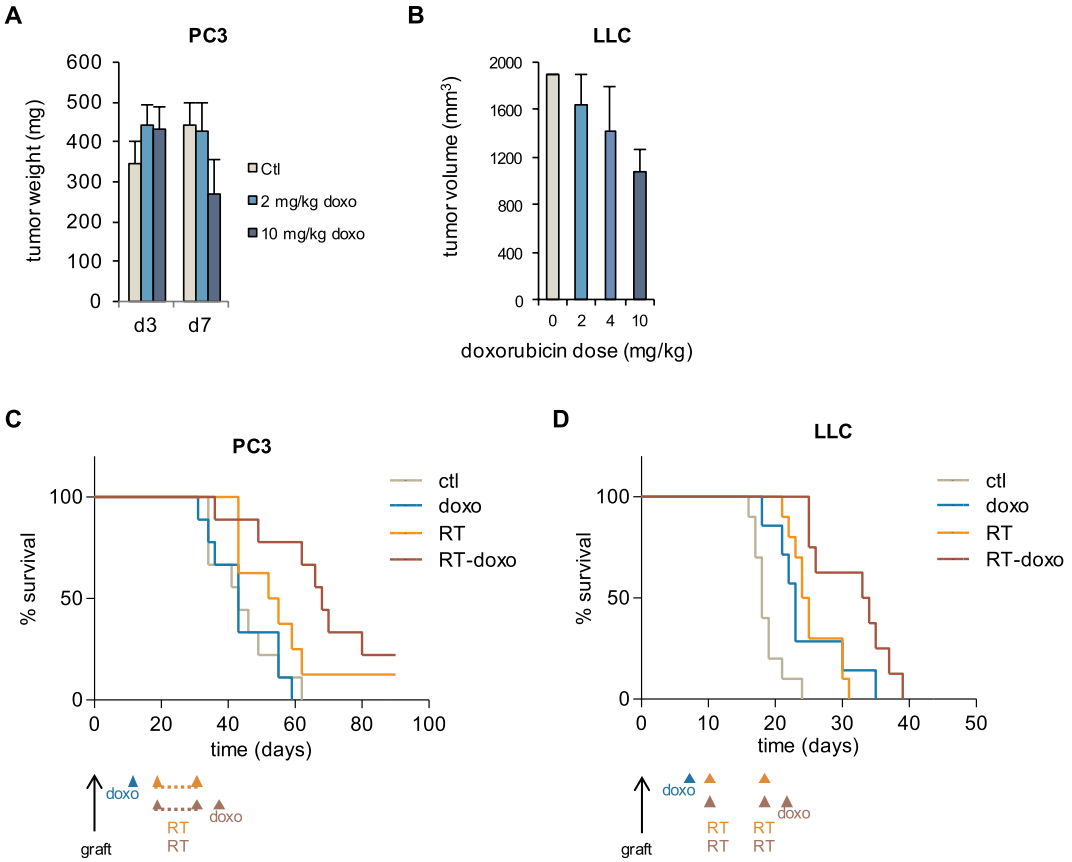

Fig. 7. RT improves drug efficacy. PC3 tumors were engrafted subcutaneously in NMRInu mice LLC tumors were engrafted subcutaneously in C57B/L6 mice. (A, B) tumor size of PC3 (A) and LLC (B) tumors one week after treatment with increasing doxorubicin doses i.p. Values represent the average of n = 3 ± sem. No statistical relevance was looked for to maintain small group size. (C, D) Animals were irradiated at 10 × 2 Gy (PC3) or 2 × 12 Gy(LLC) for two weeks, treated with doxorubicin i.p. alone, or treated with doxorubicin after RT. pseudo-survival curves (time to 2000 mm^3, Kaplan-Meier analysis) of PC3 (C) and LLC (D) tumors treated by doxorubicin alone, RT and doxorubicin 3 days after RT. (C, D) Values represent the average of n ≥ 8 per group.

hypoxia and enhancement of perfusion [17]. Similar findings were reported by Lan et al. (2013) after 3 × 12 Gy [35] and Chen et al. (2013) after 15 × 4 Gy [38]. In this study, we found several parameters indicative of vascular normalization in most of the prostate PC3, LNCaP and lung LLC models, including reduced pimonidazole retention (hypoxia) and increased Hoechst and doxorubicin distribution after doses of 10 × 2 Gy or 2 × 12 Gy. Only hypoxia was not affected in the fast proliferating LLC model although it has been reported to be reduced in smaller tumors, more affected by RT [35]. Collectively, these data argue that radiotherapy-induced vascular remodeling is a common response, with some minor variations in the phenotype.

Vascular normalization was originally reported as a transient phenomenon [39]. This is of particular interest when considering potential clinical applications. We have found that RT initiates changes starting at one week of RT and becomes more evident after the second week [17]. Similar findings have been made by independent laboratories [34,35,38]. We show here that chemotherapy delivery is more efficient at two weeks of RT, a timing that seems concordant throughout independent studies.

Pericytes belong to a versatile cell population whose function and origin is still under debate [40,41]. Their interaction with endothelial cells is dynamic during vascular development and maturation [42]. Experiments in conditional depletion models have shown that lack of pericytes impairs vascular function and favors metastasis [9,11]. Whether pericytes contribute to upregulating perfusion in a radiotherapy context is not completely elucidated, although deprivation using AMD3100 reinduced hypoxia [38]. However, given the specificity of sunitinib, PDGFRs may not be involved in RIVR. The function of pericytes in regulating blood flow is currently questioned [43]. Moreover, despite inducing hypoxia, AMD3100 delayed tumor growth. So, pericytes may exhibit ambivalent roles in facilitating drug delivery and reoxygenation while maintaining blood vessel function to support tumor growth [44]. Further studies will be needed to better characterize the impact of mural cells in the tumor response to radiotherapy.

Funding

This work was supported by Association pour la Recherche sur le Cancer, Ligue contre le Cancer, Institut National du Cancer, Fondation Mustière, Club de l'âge d'or, Transports Loizeau and ECF.

Conflicts of interest

The authors claim no potential conflicts of interest.

Acknowledgements

We thank Sylvia Lambot and UTE IRS-UN for technical help with animal experiments, Stéphanie Blandin and MicroPIcell for assistance with histology.

Appendix A. Supplementary data

Supplementary data to this article can be found online at https://doi.org/10.1016/j.canlet.2019.05.005.

References

[1] M.W. Dewhirst, T.W. Secomb, Transport of drugs from blood vessels to tumour tissue, Nat. Rev. Canc. 17 (2017) 738–750.
[2] S. Goel, D.G. Duda, L. Xu, L.L. Munn, Y. Boucher, D. Fukumura, R.K. Jain, Normalization of the vasculature for treatment of cancer and other diseases, Physiol. Rev. 91 (2011) 1071–1121.
[3] J.A. Nagy, S.H. Chang, S.C. Shih, A.M. Dvorak, H.F. Dvorak, Heterogeneity of the tumor vasculature, Semin. Thromb. Hemost. 36 (2010) 321–331.
[4] J.D. Martin, D. Fukumura, D.G. Duda, Y. Boucher, R.K. Jain, Reengineering the tumor microenvironment to alleviate hypoxia and overcome cancer heterogeneity, Cold Spring Harbor Perspect. Med. 6 (2016).
[5] R.G. Bristow, R.P. Hill, Hypoxia and metabolism. Hypoxia, DNA repair and genetic instability, Nat. Rev. Canc. 8 (2008) 180–192.
[6] R.K. Jain, Normalization of tumor vasculature: an emerging concept in anti-angiogenic therapy, Science 307 (2005) 58–62.
[7] R.N. Gacche, Compensatory angiogenesis and tumor refractoriness, Oncogenesis 4 (2015) e153.
[8] R.K. Jain, D.G. Duda, J.W. Clark, J.S. Loeffler, Lessons from phase III clinical trials on anti-VEGF therapy for cancer, Nature clinical practice, Oncology 3 (2006) 24–40.
[9] V.G. Cooke, V.S. LeBleu, D. Keskin, Z. Khan, J.T. O'Connell, Y. Teng, M.B. Duncan, L. Xie, G. Maeda, S. Vong, H. Sugimoto, R.M. Rocha, A. Damascena, R.R. Brentani, R. Kalluri, Pericyte depletion results in hypoxia-associated epithelial-to-mesenchymal transition and metastasis mediated by met signaling pathway, Cancer Cell 21 (2012) 66–81.
[10] J.M. Ebos, C.R. Lee, W. Cruz-Munoz, G.A. Bjarnason, J.G. Christensen, R.S. Kerbel, Accelerated metastasis after short-term treatment with a potent inhibitor of tumor angiogenesis, Cancer Cell 15 (2009) 232–239.
[11] D. Keskin, J. Kim, V.G. Cooke, C.C. Wu, H. Sugimoto, C. Gu, M. De Palma, R. Kalluri, V.S. LeBleu, Targeting vascular pericytes in hypoxic tumors increases lung metastasis via angiopoietin-2, Cell Rep. 10 (2015) 1066–1081.
[12] M. Paez-Ribes, E. Allen, J. Hudock, T. Takeda, H. Okuyama, F. Vinals, M. Inoue, G. Bergers, D. Hanahan, O. Casanovas, Antiangiogenic therapy elicits malignant progression of tumors to increased local invasion and distant metastasis, Cancer Cell 15 (2009) 220–231.
[13] A.M. Al-Abd, A.J. Alamoudi, A.B. Abdel-Naim, T.A. Neamatallah, O.M. Ashour, Anti-angiogenic agents for the treatment of solid tumors: potential pathways, therapy and current strategies - a review, J. Adv. Res. 8 (2017) 591–605.
[14] D. Huang, H. Lan, F. Liu, S. Wang, X. Chen, K. Jin, X. Mou, Anti-angiogenesis or pro-angiogenesis for cancer treatment: focus on drug distribution, Int. J. Clin. Exp. Med. 8 (2015) 8369–8376.
[15] J.M. Borras, Y. Lievens, P. Dunscombe, M. Coffey, J. Malicki, J. Corral, C. Gasparotto, N. Defourny, M. Barton, R. Verhoeven, L. van Eycken, M. Primic-Zakelj, M. Trojanowski, P. Strojan, C. Grau, The optimal utilization proportion of external beam radiotherapy in European countries: an ESTRO-HERO analysis, Radiotherapy and oncology, J. Eur. Soc. Ther. Radiol. Oncol. 116 (2015) 38–44.
[16] M. Garcia-Barros, F. Paris, C. Cordon-Cardo, D. Lyden, S. Rafii, A. Haimovitz-Friedman, Z. Fuks, R. Kolesnick, Tumor response to radiotherapy regulated by endothelial cell apoptosis, Science 300 (2003) 1155–1159.
[17] V.A. Potiron, R. Abderrahmani, K. Clement-Colmou, S. Marionneau-Lambot, T. Oullier, F. Paris, S. Supiot, Improved functionality of the vasculature during conventionally fractionated radiation therapy of prostate cancer, PLoS One 8 (2013) e84076.
[18] D.B. Pink, W. Schulte, M.H. Parseghian, A. Zijlstra, J.D. Lewis, Real-time visualization and quantitation of vascular permeability in vivo: implications for drug delivery, PLoS One 7 (2012) e33760.
[19] K.J. Patel, O. Tredan, I.F. Tannock, Distribution of the anticancer drugs doxorubicin, mitoxantrone and topotecan in tumors and normal tissues, Cancer Chemother. Pharmacol. 72 (2013) 127–138.
[20] S.J. Kim, K.H. Jung, M.K. Son, J.H. Park, H.H. Yan, Z. Fang, Y.W. Kang, B. Han, J.H. Lim, S.S. Hong, Tumor vessel normalization by the PI3K inhibitor HS-173 enhances drug delivery, Cancer Lett. 403 (2017) 339–353.
[21] N. Qayum, J. Im, M.R. Stratford, E.J. Bernhard, W.G. McKenna, R.J. Muschel, Modulation of the tumor microvasculature by phosphoinositide-3 kinase inhibition increases doxorubicin delivery in vivo, Clin. Cancer Res. : Off. J. Am. Assoc. Cancer Res. 18 (2012) 161–169.
[22] C.M. Ma, C.W. Coffey, L.A. DeWerd, C. Liu, R. Nath, S.M. Seltzer, J.P. Seuntjens, M. American Association of Physicists, AAPM protocol for 40-300 kV x-ray beam dosimetry in radiotherapy and radiobiology, Med. Phys. 28 (2001) 868–893.
[23] C. Noblet, S. Chiavassa, F. Paris, S. Supiot, A. Lisbona, G. Delpon, Underestimation of dose delivery in preclinical irradiation due to scattering conditions, Physica medica : PM : an international journal devoted to the applications of physics to medicine and biology, Off. J. Ital. Assoc. Biomed. Phys. 30 (2014) 63–68.
[24] J.V. Gaustad, T.G. Simonsen, M.N. Leinaas, E.K. Rofstad, Sunitinib treatment does not improve blood supply but induces hypoxia in human melanoma xenografts, BMC Canc. 12 (2012) 388.
[25] D.B. Mendel, A.D. Laird, X. Xin, S.G. Louie, J.G. Christensen, G. Li, R.E. Schreck, T.J. Abrams, T.J. Ngai, L.B. Lee, L.J. Murray, J. Carver, E. Chan, K.G. Moss, J.O. Haznedar, J. Sukbuntherng, R.A. Blake, L. Sun, C. Tang, T. Miller, S. Shirazian, G. McMahon, J.M. Cherrington, In vivo antitumor activity of SU11248, a novel tyrosine kinase inhibitor targeting vascular endothelial growth factor and platelet-derived growth factor receptors: determination of a pharmacokinetic/pharmacodynamic relationship, Clin. Cancer Res. : Off. J. Am. Assoc. Cancer Res. 9 (2003) 327–337.
[26] C. Brooks, T. Sheu, K. Bridges, K. Mason, D. Kuban, P. Mathew, R. Meyn, Preclinical evaluation of sunitinib, a multi-tyrosine kinase inhibitor, as a radiosensitizer for human prostate cancer, Radiat. Oncol. 7 (2012) 154.
[27] J.K. Saggar, A.S. Fung, K.J. Patel, I.F. Tannock, Use of molecular biomarkers to quantify the spatial distribution of effects of anticancer drugs in solid tumors, Mol. Cancer Ther. 12 (2013) 542–552.
[28] L. Davies Cde, L.M. Lundstrom, J. Frengen, L. Eikenes, S.O. Bruland, O. Kaalhus, M.H. Hjelstuen, C. Brekken, Radiation improves the distribution and uptake of liposomal doxorubicin (caelyx) in human osteosarcoma xenografts, Cancer Res. 64 (2004) 547–553.
[29] H. Kalofonos, G. Rowlinson, A.A. Epenetos, Enhancement of monoclonal antibody uptake in human colon tumor xenografts following irradiation, Cancer Res. 50 (1990) 159–163.
[30] T. Barrett, M. Brechbiel, M. Bernardo, P.L. Choyke, MRI of tumor angiogenesis, J. Magn. Reson. Imaging : JMRI 26 (2007) 235–249.
[31] S. Supiot, C. Rousseau, M. Dore, C. Cheze-Le-Rest, C. Kandel-Aznar, V. Potiron, S. Guerif, F. Paris, L. Ferrer, L. Campion, P. Meingan, G. Delpon, M. Hatt, D. Visvikis, Evaluation of tumor hypoxia prior to radiotherapy in intermediate-risk prostate cancer using (18)F-fluoromisonidazole PET/CT: a pilot study, Oncotarget 9 (2018) 10005–10015.
[32] P.L. Debbage, S. Seidl, A. Kreczy, P. Hutzler, M. Pavelka, P. Lukas, Vascular permeability and hyperpermeability in a murine adenocarcinoma after fractionated radiotherapy: an ultrastructural tracer study, Histochem. Cell Biol. 114 (2000) 259–275.
[33] A. Maeda, Y. Chen, J. Bu, H. Mujcic, B.G. Wouters, R.S. DaCosta, Vivo imaging reveals significant tumor vascular dysfunction and increased tumor hypoxia-inducible factor-1alpha expression induced by high single-dose irradiation in a pancreatic tumor model, Int. J. Radiat. Oncol. Biol. Phys. 97 (2017) 184–194.
[34] F.H. Chen, C.S. Chiang, C.C. Wang, C.S. Tsai, S.M. Jung, C.C. Lee, W.H. McBride, J.H. Hong, Radiotherapy decreases vascular density and causes hypoxia with macrophage aggregation in TRAMP-C1 prostate tumors, Clin. Cancer Res. : Off. J. Am. Assoc. Cancer Res. 15 (2009) 1721–1729.
[35] J. Lan, X.L. Wan, L. Deng, J.X. Xue, L.S. Wang, M.B. Meng, H. Ling, X. Zhang, X.M. Mo, Y. Lu, Ablative hypofractionated radiotherapy normalizes tumor vasculature in lewis lung carcinoma mice model, Radiat. Res. 179 (2013) 458–464.
[36] V.P. Chauhan, J.D. Martin, H. Liu, D.A. Lacorre, S.R. Jain, S.V. Kozin, T. Stylianopoulos, A.S. Mousa, X. Han, P. Adstamongkonkul, Z. Popovic, P. Huang, M.G. Bawendi, Y. Boucher, R.K. Jain, Angiotensin inhibition enhances drug delivery and potentiates chemotherapy by decompressing tumour blood vessels, Nat. Commun. 4 (2013) 2516.
[37] S.J. Lunt, A. Fyles, R.P. Hill, M. Milosevic, Interstitial fluid pressure in tumors: therapeutic barrier and biomarker of angiogenesis, Future Oncol. 4 (2008) 793–802.
[38] F.H. Chen, S.Y. Fu, Y.C. Yang, C.C. Wang, C.S. Chiang, J.H. Hong, Combination of vessel-targeting agents and fractionated radiation therapy: the role of the SDF-1/CXCR4 pathway, Int. J. Radiat. Oncol. Biol. Phys. 86 (2013) 777–784.
[39] F. Winkler, S.V. Kozin, R.T. Tong, S.S. Chae, M.F. Booth, I. Garkavtsev, L. Xu, D.J. Hicklin, D. Fukumura, E. di Tomaso, L.L. Munn, R.K. Jain, Kinetics of vascular normalization by VEGFR2 blockade governs brain tumor response to radiation: role of oxygenation, angiopoietin-1, and matrix metalloproteinases, Cancer Cell 6 (2004) 553–563.
[40] P.H. Dias Moura Prazeres, I.F.G. Sena, I.D.T. Borges, P.O. de Azevedo, J.P. Andreotti, A.E. de Paiva, V.M. de Almeida, D.A. de Paula Guerra, G.S. Pinheiro Dos Santos, A. Mintz, O. Delbono, A. Birbrair, Pericytes are heterogeneous in their origin within the same tissue, Dev. Biol. 427 (2017) 6–11.
[41] A. Holm, T. Heumann, H.G. Augustin, Microvascular mural cell organotypic heterogeneity and functional plasticity, Trends Cell Biol. 28 (4) (April 1, 2018) 302–316.
[42] A.A. Berthiaume, R.I. Grant, K.P. McDowell, R.G. Underly, D.A. Hartmann, M. Levy, N.R. Bhat, A.Y. Shih, Dynamic remodeling of pericytes in vivo maintains capillary coverage in the adult mouse brain, Cell Rep. 22 (2018) 8–16.
[43] R.A. Hill, L. Tong, P. Yuan, S. Murikinati, S. Gupta, J. Grutzendler, Regional blood flow in the normal and ischemic brain is controlled by arteriolar smooth muscle cell contractility and not by capillary pericytes, Neuron 87 (2015) 95–110.
[44] R. Hamdan, Z. Zhou, E.S. Kleinerman, Blocking SDF-1alpha/CXCR4 downregulates PDGF-B and inhibits bone marrow-derived pericyte differentiation and tumor vascular expansion in Ewing tumors, Mol. Cancer Ther. 13 (2014) 483–491.